

circRNAome profiling reveals circFgfr2 regulates myogenesis and muscle regeneration via a feedback loop

Junyu Yan^{1,2,3†}, Yalan Yang^{1,2,3†}, Xinhao Fan^{1,2,3}, Guoming Liang³, Zishuai Wang^{1,2,3}, Jiju Li^{1,2,3}, Liyuan Wang^{1,2,3}, Yun Chen^{1,2,3}, Adeyinka Abiola Adetula^{1,2,3}, Yijie Tang^{1,2,3}, Kui Li^{1,2,3}, Dazhi Wang⁴ & Zhonglin Tang^{1,2,3,5,6*}

¹Shenzhen Branch, Guangdong Laboratory for Lingnan Modern Agriculture, Agricultural Genomics Institute at Shenzhen, Chinese Academy of Agricultural Sciences, Shenzhen, China; ²Genome Analysis Laboratory of the Ministry of Agriculture and Rural Affairs, Agricultural Genomics Institute at Shenzhen, Chinese Academy of Agricultural Sciences, Shenzhen, China; ³Research Centre of Animal Nutritional Genomics, State Key Laboratory of Animal Nutrition, Institute of Animal Sciences, Chinese Academy of Agricultural Sciences, Shenzhen, China; ⁴Department of Cardiology, Boston Children's Hospital, Harvard Medical School, Boston, MA, USA; ⁵GuangXi Engineering Centre for Resource Development of Bama Xiang Pig, Bama, China; ⁶Kunpeng Institute of Modern Agriculture at Foshan, Foshan, China

Abstract

Background Circular RNAs (circRNAs) represent a novel class of non-coding RNAs formed by a covalently closed loop and play crucial roles in many biological processes. Several circRNAs associated with myogenesis have been reported. However, the dynamic expression, function, and mechanism of circRNAs during myogenesis and skeletal muscle development are largely unknown.

Methods Strand-specific RNA-sequencing (RNA-seq) and microarray datasets were used to profile the dynamic circRNAome landscape during skeletal muscle development and myogenic differentiation. Bioinformatics analyses were used to characterize the circRNAome and identify candidate circRNAs associated with myogenesis. Bulk and single-cell RNA-seq were performed to identify the downstream genes and pathways of circFgfr2. The primary myoblast cells, C2C12 cells, and animal model were used to assess the function and mechanism of circFgfr2 in myogenesis and muscle regeneration *in vitro* or *in vivo* by RT-qPCR, western blotting, dual-luciferase activity assay, RNA immunoprecipitation, RNA fluorescence *in situ* hybridization, and chromatin immunoprecipitation.

Results We profiled the dynamic circRNAome in pig skeletal muscle across 27 developmental stages and detected 52 918 high-confidence circRNAs. A total of 2916 of these circRNAs are conserved across human, mouse, and pig, including four circRNAs (circFgfr2, circQrich1, circMettl9, and circCamta1) that were differentially expressed ($|\log_2$ fold change| > 1 and adjusted *P* value < 0.05) in various myogenesis systems. We further focused on a conserved circRNA produced from the fibroblast growth factor receptor 2 (Fgfr2) gene, termed circFgfr2, which was found to inhibit myoblast proliferation and promote differentiation and skeletal muscle regeneration. Mechanistically, circFgfr2 acted as a sponge for miR-133 to regulate the mitogen-activated protein kinase kinase kinase 20 (Map3k20) gene and JNK/MAPK pathway. Importantly, transcription factor Kruppel like factor 4 (Klf4), the downstream target of the JNK/MAPK pathway, directly bound to the promoter of circFgfr2 and affected its expression via an miR-133/Map3k20/JNK/Klf4 auto-regulatory feedback loop. RNA binding protein G3BP stress granule assembly factor 1 (G3bp1) inhibited the biogenesis of circFgfr2.

Conclusions The present study provides a comprehensive circRNA resource for skeletal muscle study. The functional and mechanistic analysis of circFgfr2 uncovered a circRNA-mediated auto-regulatory feedback loop regulating myogenesis and muscle regeneration, which provides new insight to further understand the regulatory mechanism of circRNAs.

Keywords circRNA; circFgfr2; Skeletal muscle; Development; Regeneration; Feedback loop

Received: 20 April 2021; Revised: 15 October 2021; Accepted: 19 October 2021

*Correspondence to: Zhonglin Tang, Agricultural Genomics Institute at Shenzhen, Chinese Academy of Agricultural Sciences, Shenzhen 518124, China. Tel: 86-0755-23251432. Email: tangzhonglin@caas.cn

[†]These two authors contributed equally to this work.

Introduction

Skeletal muscle is the most abundant tissue in humans and other mammals of normal weight. The generation of skeletal muscle during embryonic development and postnatal regeneration relies on myogenesis,^{1,2} which is a highly orchestrated process composed of the determination of multipotential mesodermal cells, myoblast proliferation and migration, fusion of myocytes into multinucleated myofibres, and maturation of the muscle fibre.^{3,4} These processes are tightly and sophisticatedly controlled by the expression of myogenic genes such as myogenic regulatory factors (MRFs) and paired box (PAX) genes.^{5–7} Meanwhile, non-coding RNAs (ncRNAs), such as microRNAs (miRNAs) and long non-coding RNAs (lncRNAs), are emerging as regulators of skeletal muscle development and regeneration.^{8–10} For instance, our previous study suggested that miR-148a promotes myogenic differentiation of both C2C12 myoblasts and primary muscle cells by targeting the Rho-associated, coiled-coil-containing protein kinase 1 (ROCK1) gene.⁹

Circular RNAs (circRNAs) are a new type of endogenous ncRNA covalently closed by a non-canonical splicing event called backsplicing.^{11–13} In recent years, owing to the development of high-throughput RNA sequencing (RNA-seq) and specific bioinformatics algorithms for circRNAs, thousands of circRNAs have been identified in eukaryotes including humans, mice, pigs, and chickens.^{14–18} Mounting evidence suggests that circRNAs play important roles in development and disease.¹³ To date, only a few circRNAs associated with myogenesis have been functionally and mechanistically characterized, and these typically act as molecular sponges for specific miRNAs, regulating the expression of muscle-related genes via the competing endogenous RNA (ceRNA) mechanism.^{19–22} For instance, circLMO7 regulates myoblast differentiation and survival by sponging miR-378a-3p.¹⁹ In addition to the sponge effect, other regulatory mechanisms of circRNAs in myogenesis have also been proposed. circZNF609, which is translated into protein in a splicing-dependent and cap-independent manner, controls myoblast proliferation.²³ Despite these progresses, the dynamic expression of circRNAs during skeletal muscle development remains largely unclear and their roles in myogenesis and muscle regeneration require further systematic exploration.

The pig is an outstanding model organism for the study of human development and disease.^{24–27} Recently, we generated the transcriptome landscape of skeletal muscle across 27 developmental stages using Ribo-Zero strand-specific RNA-seq in pig.²⁸ These datasets provide rich information for studying the function and regulation of non-coding RNAs

such as circRNA in skeletal muscle development. In the present study, with a view to systematically identifying circRNAs associated with myogenesis, we profiled the circRNAome landscape of skeletal muscle using these datasets and identified 52 918 high-confidence circRNAs. Analysis of these circRNAs revealed that many are conserved across species and differentially expressed during skeletal muscle development and myoblast differentiation. Fibroblast growth factor receptor 2 (Fgfr2) is an important stimulatory modulator of satellite cells and is essential for the maintenance and repair of skeletal muscle.²⁹ We further characterized one conserved circRNA produced from the Fgfr2 gene, termed circFgfr2, which was differentially expressed during skeletal muscle development and was up-regulated during myogenic differentiation. Functional studies *in vitro* (mouse C2C12 cells and primary myoblasts) and *in vivo* revealed that circFgfr2 regulated myogenesis and muscle regeneration by acting as a sponge for miR-133. We revealed a new Klf4-mediated feedback loop between circFgfr2 and the JNK/MAPK pathway involving an exquisite mechanism for regulating myogenesis. Our findings provide a comprehensive circRNA resource for studying muscle development and demonstrate a circRNA-mediated auto-regulatory feedback loop regulating myogenesis.

Materials and methods

Identification of circRNAs in skeletal muscle

The Ribo-Zero strand-specific RNA-seq data used for circRNA identification were obtained from our previous studies (GEO accession number GSE157044).^{28,30} The transcriptome data were generated from the skeletal muscle of Landrace pigs at 27 developmental stages from embryonic day 33 (E33) to postnatal day 180 (D180). The corresponding whole-genome bisulfite sequencing (WGBS) data (GEO accession number GSE157043) were used to evaluate the methylation level across the circRNAs. Further details on identification and characteristics analysis of circRNAs are provided in the Supporting Information, *Data S1*.

Animal studies

C57BL/6 male mice were purchased from the Charles River Labs (Beijing, China) and maintained in our laboratory. All animal procedures were performed according to the protocols of the Chinese Academy of Agricultural Sciences and the

Institutional Animal Care and Use Committee. No drug tests were carried out. For cardiotoxin (CTX) administration, adenoviruses expressing circFgfr2 (10^{10} – 10^{11} p.f.u./mL) were injected into the tibialis anterior (TA) muscles of 6-week-old C57BL/6 mice. After 28 days, the mice were injected with 100 μ L CTX (10 μ M) at the same place. Mice were sacrificed and TA muscles were collected at different time points after CTX injury. For further details, see *Data S1*.

Cell isolation and culture

Mouse primary myoblasts, HEK293T and C2C12 cells, were used in this study. Mouse primary myoblasts were isolated from the TA muscles of newborn C57BL/6 mice. The primary myoblasts were cultured in Ham's F10 nutrient medium (Gibco) supplemented with 20% fetal bovine serum (Gibco) and 5 ng/mL basic fibroblast growth factor. HEK293T and C2C12 cells were cultured as previously described.²⁸ For further details, see *Data S1*.

Plasmid construction and RNA interference

To construct the circFgfr2-overexpression vector, the full-length sequence of mouse circFgfr2 was cloned into the pLCDH-ciR vector (Geenseed Biotech, Guangzhou, China). To knock down circFgfr2, three siRNAs (si-circFgfr2-1, -2, and -3) targeting the back-splicing junction (BSJ) of circFgfr2 and a negative control (siRNA-NC) were synthesized (RiboBio Biotech, Guangzhou, China). The plasmid construction and siRNAs of other genes are described in *Data S1*.

circRNA microarray analysis

The circRNA microarray was analysed using the Arraystar Mouse circRNA Array V2 (Arraystar, Rockville, MD, USA). After quantile normalization of the raw data, the differentially expressed circRNAs with statistical significance were identified using a Student's *t*-test with a cut-off value for false discovery rate (FDR) ≤ 0.05 and an absolute fold change (FC) ≥ 2 . For further details, see *Data S1*.

RNA-sequencing analysis

The RNA-seq libraries were prepared using the NEBNext Ultra RNA Library Prep Kit for Illumina (NEB, USA) according to the manufacturer's instructions and were sequenced on an Illumina NovaSeq platform to generate 150 bp paired-end reads. The bioinformatics analysis of the RNA-seq data was performed as described previously.^{28,30} For further details, see *Data S1*.

Single-cell RNA-sequencing analysis

Library construction and single-cell RNA-seq were performed according to the instructions of the Chromium Next GEM Single Cell 3 Reagent Kit v3.1. Sequencing reads were processed by Cell Ranger version 3.0.1 (10x Genomics, Pleasanton, CA, USA) using the mouse reference transcriptome mm10. Quality control, filtering, data clustering, data visualization, and differential expression analysis were performed using Seurat version 2.3.4 R package.³¹ For further details, see *Data S1*.

Cell proliferation and cell cycle assay

Cell proliferation was assessed using the Cell-Light EdU DNA cell proliferation kit (RiboBio) and Cell Counting Kit-8 (CCK-8) (Dojindo) according to the manufacturer's instructions. Flow cytometry analysis of the cell cycle was performed on a BD Accuri C6 flow cytometer (BD Biosciences, San Jose, CA, USA) as previously described,¹⁸ and data were processed using the FlowJo7.6 software (Treestar Incorporated, Ashland, OR, USA).

RNA preparation and RT-qPCR

Total RNA was extracted using TRIzol reagent (Invitrogen), and cDNAs were prepared using reverse transcriptase (Thermo Fisher Scientific). RT-qPCR data were analysed using the $\Delta\Delta$ Ct method, and individual gene expression was normalized to GAPDH RNA expression. The primer sequences used in the present study are listed in *Table S1*. For further details, see *Data S1*.

Western blotting and chromatin immunoprecipitation

Western blotting was performed as described previously.^{30,32} Band intensities were quantified using the ImageJ program, normalized relative to the quantity of their respective internal bands, and expressed as percentages of the strongest value. The following dilutions were used for each antibody: myogenin(1:1000; ProteinTech), MyHC1 (1:1000; DSHB), Ki67 (1:1000; Abcam), MyoD (1:1000; ProteinTech), Pax7 (1:1000; ProteinTech), GAPDH (1:1000; ProteinTech), tubulin (1:1000; ProteinTech), MKK7 (1:1000; CST), p-MKK7 (1:1000; CST), JNK (1:1000; CST), and p-JNK (1:1000; CST). Chromatin immunoprecipitation (ChIP) was performed using a ChIP Assay Kit (EMD Millipore Corporation, Billerica, MA, USA) as described previously.²⁸

Other molecular experiments

The procedures used for histology, RNA-FISH, immunohistochemistry, immunostaining RNA immunoprecipitation (RIP), and other assays are described in the *Data S1*.

Data availability

All microarray expression, and RNA-seq and scRNA-seq data have been deposited in the China National GenBank (CNCB; <https://db.cngb.org/>) Nucleotide Sequence Archive (CNSA) under accession number CNP0001431.

Results

CircRNAome profiling of skeletal muscle across 27 developmental stages

To characterize the landscape of circRNA profiles in skeletal muscle, we analysed an extensive RNA-sequencing (RNA-

seq) dataset (GSE157044) that covers the 27 developmental stages of skeletal muscle and annotated a total of 104 896 circRNAs, which contained at least 2 unique back-spliced reads. CircRNAs were considered robustly expressed when detected in a minimum of five distinct samples, resulting in a total of 52 918 high-confidence circRNAs for downstream analysis (*Figure 1A*, *Table S2*). To validate the reliability of these circRNAs, 45 were chosen and confirmed by PCR using reverse transcription (RT-PCR) with divergent primers. BSJ was successfully detected in 43 of 45 (95.56%) circRNA candidates and confirmed by Sanger sequencing (*Table S3*). RT-PCR of the total RNase R-treated RNA showed that these circRNAs were resistant to digestion, validating the circularity of circRNAs (*Figures 1B* and *S1*).

Most circRNAs were located in exons (46 549), followed by intronic (4759), intergenic (1155), and antisense (455) circRNAs (*Figure 1C*). In comparison with the known pig circRNAs reported in the circAtlas database,³³ we found that 41.12% (21 761/52 918) of the identified circRNAs were novel, which greatly expands the catalogue of pig circRNAs (*Figure 1D*, *Table S3*). Characteristics analysis showed that the median exon number and length of the exonic circRNAs were 4 (*Figure 1E*) and 581 bp (*Figure 1F*), respectively,

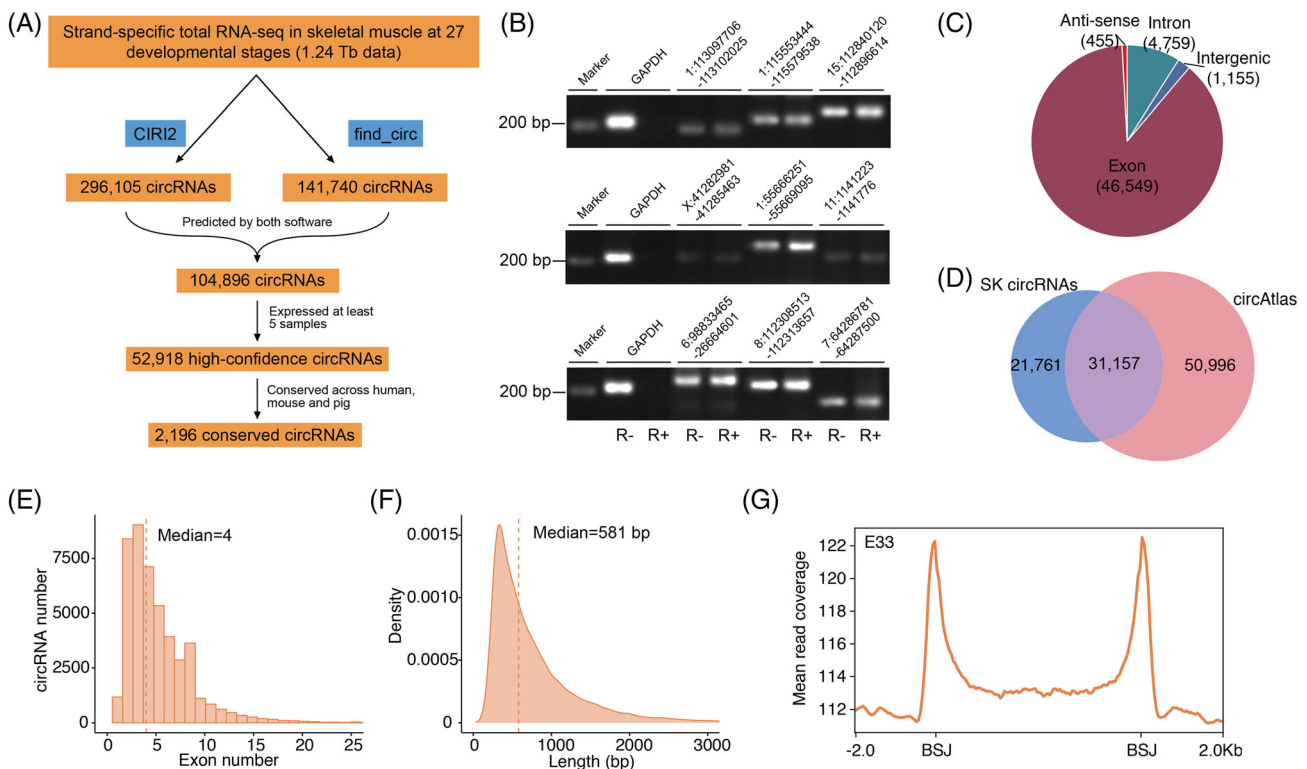


Figure 1 Identification and characteristics of circRNAs in pig skeletal muscle. (A) Pipeline for the identification of novel circRNAs. (B) Validation of the circularity of circRNAs. RT-PCR to detect circRNAs was performed on mock-treated and RNase R-treated RNA using divergent primers. Linear GAPDH mRNA was used as a negative control. (C) Distribution of circRNAs in different genomic regions. (D) Venn diagram showing the overlap between circRNAs that we identified and pig circRNAs deposited in the circAtlas database. (E) The exon number distribution of identified circRNAs. (F) The length distribution of identified circRNAs. (G) Average read coverage of DNA methylation across gene bodies and the 2 kb regions flanking the BSJ sites of circRNAs at the E33 stage.

similar to previous reports in pigs.¹⁶ Meanwhile, 72.76% (5312/7301) of the host genes corresponding to exonic circRNAs could produce at least 2 circRNAs (Figure S2A). Although the expression of most circRNAs was restricted to a subset of samples, we observed a subset of circRNAs ($n = 3552$) that was widely expressed (in at least 80% samples) in skeletal muscle (Figure S2B). We noticed that the gene body of circRNAs had a higher methylation level than that of neighbouring regions. Interestingly, we observed a marked hypermethylation around BSJ sites (Figures 1G and S3). We subsequently identified 12 677 and 4792 conserved circRNAs between pig and human and between pig and mouse, respectively. Among them, 2916 circRNAs were conserved across pig, human, and mouse (Table S2).

Dynamic temporal regulation of circRNAs during skeletal muscle development

We identified 9848–19 506 circRNAs expressed in each skeletal muscle, with many more circRNAs being expressed in prenatal than postnatal muscle (Figure 2A). Cluster analysis based on the expression of circRNAs clearly classified the skeletal muscle samples into prenatal and postnatal groups (Figure S4). Principal components analysis (PCA) revealed the overall pattern of circRNA expression was highly developmentally dependent, being ordered from embryonic to adult stages during skeletal muscle development (Figure 2B). These results suggest that circRNAs were dynamically expressed in a temporally dependent manner during skeletal muscle development.

To detect circRNAs that were temporally regulated during skeletal muscle development, a total of 7198 differentially expressed circRNAs (DECs) were identified between any two stages ($\log_2 FC \geq 1$ and $FDR \leq 0.05$; Table S4), accounting for 13.60% (7198/52 918) of all expressed circRNAs (Figure 2C). In comparison with exonic non-DECs, exonic DECs had a shorter transcript length (Figure 2D) and a lower exon number (Figure 2E). Subsequently, we performed WGCNA co-expression network analysis³⁴ focusing on these DECs and revealed seven distinct co-expression modules (M1–M7; Table S4). Three clusters (M2, M3, and M6) showed dynamic temporal expression during skeletal muscle development (Figure 2F). The circRNAs in clusters M2 and M3 were abundantly expressed during the prenatal stages. The expression of circRNAs in M2 gradually increased with skeletal muscle development and those in M3 gradually decreased. Gene ontology (GO) enrichment analysis showed that the host genes in M2 were enriched for GO categories related to cellular localization and proliferation (Figure 2G). The host genes in M3 were functionally involved in embryonic morphogenesis, nervous system development, and cell differentiation (Figure 2H). The circRNAs in M6 were mainly expressed during postnatal stages and up-regulated during postnatal skeletal

muscle development. These host genes of circRNAs in M6 were significantly associated with protein catabolic and modification processes (Figure 2I).

circFgfr2 is highly conserved and a candidate regulator of skeletal muscle development

To further identify potential circRNAs involved in myogenesis, microarray analysis was carried out in mouse C2C12 myoblasts cultured in growth medium (GM) and in differentiation medium (DM). In comparison with myoblasts cultured in GM, 66 circRNAs were up-regulated in myoblasts cultured in DM ($\log_2 FC \geq 1$ and $FDR \leq 0.05$; Figure 3A and Table S5). Six up-regulated circRNAs were successfully validated by RT-qPCR using divergent primers (Figure 3B), suggesting that these DECs were reliable for further analysis. Among the 66 circRNAs, six were identical to the pig circRNAs, including four circRNAs (circFgfr2, circQrich1, circMettl9, and circCamta1) that were also differentially expressed during pig skeletal muscle development, indicating that these circRNAs may regulate mammalian skeletal muscle development in a conserved manner.

Among these four conserved DECs, circFgfr2 aroused our interest. The host gene of circFgfr2, fibroblast growth factor receptor 2 (Fgfr2), is essential for the maintenance and repair of skeletal muscle.²⁹ circFgfr2 is a stable exonic circRNA generated by exons 3–6 of the linear sequence in mice. The BSJ sequence of circFgfr2 was verified by Sanger sequencing (Figure 3C), and RT-PCR of circFgfr2 from RNase R-treated RNA showed that circFgfr2 was resistant to digestion, indicating a closed-loop structure (Figure 3D). Conservation analysis suggested that the BSJ sequences of circFgfr2 were highly conserved across humans, mice, pigs, and chickens (Figure S5).

We examined the temporal expression patterns in several myogenesis systems. The expression of circFgfr2 in mouse TA muscles was abundant during the neonatal stage and down-regulated during postnatal development (Figure 3E). During C2C12 cell differentiation, the expression of circFgfr2 was found to be increased in a time-dependent manner during the first 4 days following differentiation (Figure 3F). Meanwhile, using a well-established CTX-induced skeletal muscle damage and regeneration model (Figure S6), we found that the expression of circFgfr2 was highly induced during the first 2 days post-injury and subsequently decreased (Figure 3G). However, the temporal expression patterns of circFgfr2 were independent of the patterns of Fgfr2 (Figure S7). Meanwhile, RT-qPCR analysis revealed that circFgfr2 was enriched in fast-twitch quadriceps muscle instead of slow-twitch soleus muscle (Figure 3H), suggesting that the differential expression of circFgfr2 in different fibre types of skeletal muscles might depend on their metabolic status. Subcellular localization analysis based on FISH and

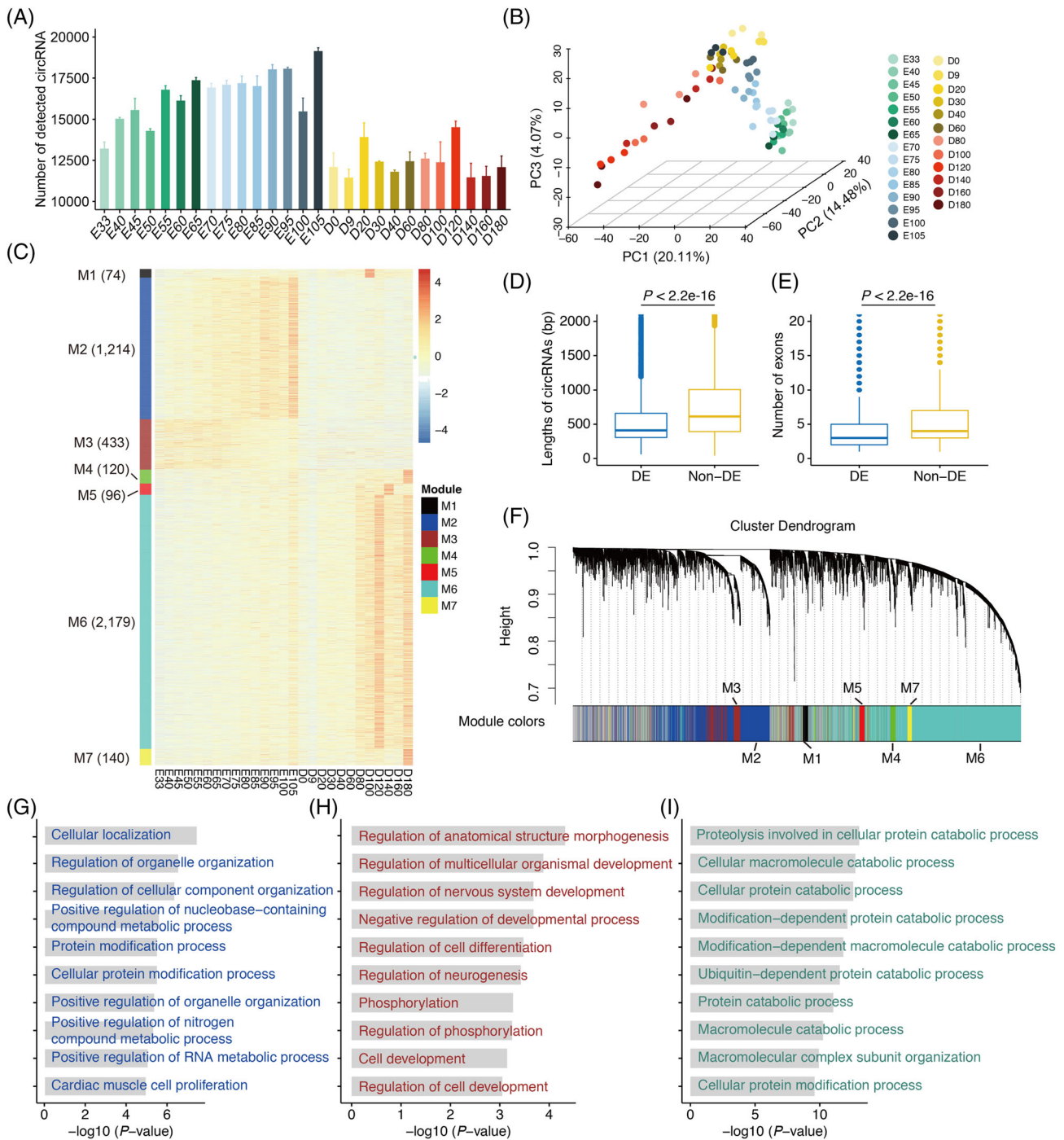


Figure 2 Dynamic expression of circRNAs during pig skeletal muscle development. (A) The number of detected circRNAs during each developmental stage. (B) PCA plot showing the global view of dynamic circRNA expression during skeletal muscle development, coloured according to developmental stage. The 3382 circRNAs that were expressed in at least 80% of samples were used for PCA analysis. (C) Heatmap showing the expression pattern of differentially expressed circRNAs (DECs) during skeletal muscle development. (D) Comparison of the transcript length between DECs and non-DECs. (E) Comparison of the exon number between DECs and non-DECs. (F) Dendrogram from WGCNA co-expression network analysis of skeletal muscle samples. Modules of co-expressed genes were assigned a colour and number (M1–M12). (G–I) GO enrichment analysis of the host genes of DECs in the M2 (G), M3 (H), and M6 (I) modules. The top 10 biological processes reported by DAVID 6.8 are shown.

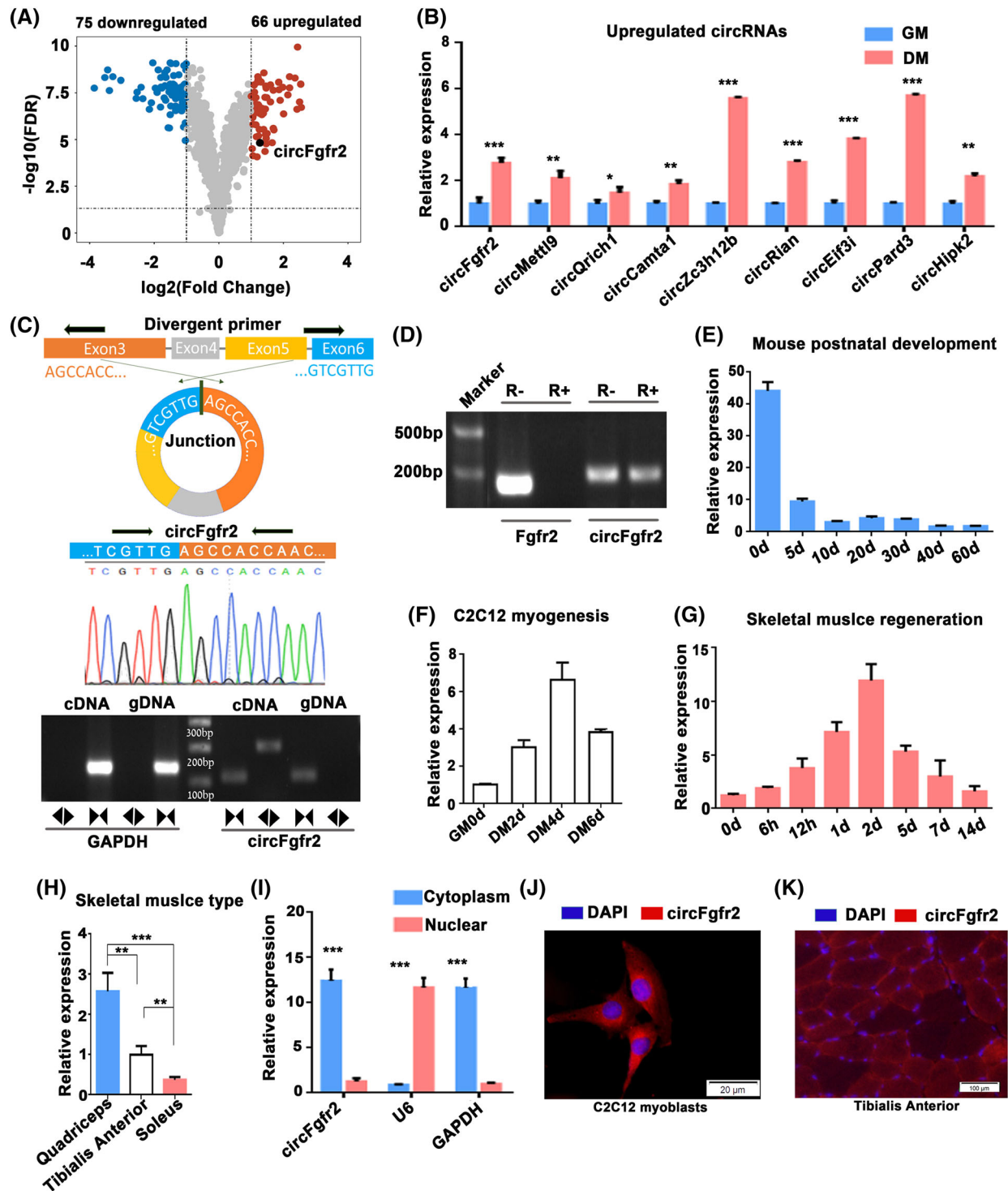


Figure 3 circFgfr2 is highly conserved and a candidate regulator of skeletal muscle development. (A) Volcano plot presents the differentially expressed circRNAs ($|\log_2 \text{fold change}| > 1$ and $\text{FDR} < 0.05$) in differentiated C2C12 myotubes (DM) as compared with myoblasts (GM). (B) Validation of up-regulated circRNAs in DM by RT-qPCR. (C) The BJS of circFgfr2 was identified using a divergent primer and sequenced by Sanger sequencing. (D) RT-PCR analysis of circFgfr2 and linear Fgfr2 mRNAs on mock-treated and RNase R-treated RNA. (E–G) RT-qPCR analysis of the expression of circFgfr2 during postnatal development in TA muscles from C57BL/6 mice (E), during C2C12 cell differentiation (F), and during CTX-induced regeneration (G). (H) The expression level of circFgfr2 in different fibre types. The expression level was normalized to 18s-ribosomal RNA. $N = 3-5$ in each group. (I) Determination of circFgfr2 localization by subcellular fractionation. The error bars depict the mean \pm SD of samples from three to five individuals. ** $P < 0.01$ and *** $P < 0.001$. (J and K) An RNA-FISH assay was performed to determine circFgfr2 subcellular localization in C2C12 myoblasts (J) and TA muscles (K). Blue indicates nuclei stained with DAPI; red indicates the RNA probe that recognizes circFgfr2. The scale of (J) is 20 μm ; (K) is 100 μm .

chromatin fractionation experiments reveal that circFgfr2 was mainly distributed in the cytoplasm (Figure 3I–3K). Taken together, these data indicate that circFgfr2 is a potential circRNA regulating myogenesis and muscle regeneration.

circFgfr2 represses myoblast proliferation and promotes myoblast differentiation and muscle regeneration

To explore the functions of circFgfr2 in myogenesis, we first investigated whether circFgfr2 affects the proliferation and differentiation of mouse myoblasts. Mouse primary myoblasts were transfected with a circFgfr2-overexpression vector and siRNAs against circFgfr2. The overexpression vector (pICDH-circFgfr2) and all three siRNAs (si-circFgfr2-1, -2, and -3) could efficiently change the expression of circFgfr2 (Figure S8), with no significant effect in the expression of linear *Fgfr2* mRNA (Figure S8C and S8F). si-circFgfr2-1 had the highest interference efficiency among the three siRNAs and was chosen for subsequent analysis (Figure S8E).

In mouse primary myoblasts and C2C12 myoblasts, both the ethynyl-2'-deoxyuridine (EdU) incorporation assay and CCK-8 assay showed that overexpression of circFgfr2 decreased cell proliferation activity (Figures 4A, 4B, and S9), and the opposite effect was observed following knockdown of circFgfr2 (Figure S9). Overexpression of circFgfr2 significantly decreased the expression of proliferation markers at both the mRNA and protein levels (Figure 4C and 4D), whereas knockdown of circFgfr2 significantly up-regulated the expression of these genes (Figure S9G and S9H). Cell cycle analysis revealed that overexpression of circFgfr2 increased the number of cells that progressed to the G0/G1 phase and reduced the number of cells that progressed to the S phase (Figure 4E and 4F), and the opposite effect was observed after circFgfr2 knockdown (Figure S9I and S9J). Meanwhile, overexpression of circFgfr2 significantly promoted the myogenic differentiation as demonstrated by the increased expression of MyHC1, MyoD, and myogenin at both the mRNA (Figure 4G) and protein levels (Figure 4H), and the immunofluorescence assay confirmed that circFgfr2 overexpression facilitated MyHC expression (Figure 4I) and myotube formation. Quantitative analysis showed that in comparison with the control, the circFgfr2 overexpression group exhibited more myotubes with multiple myonuclei (Figure 4J). Conversely, myoblast differentiation was significantly inhibited following circFgfr2 knockdown (Figure S9K–S9N).

Given that circFgfr2 was involved in myogenesis (Figure 3E–3G), we hypothesized that circFgfr2 also exerted a role in muscle regeneration *in vivo*. To validate this, TA muscles of C57BL/6 mice were injected with an adenovirus-mediated circFgfr2-overexpression vector (AAV-circFgfr2-OV) and controls (AAV-circFgfr2-NC). As expected, the expression of circFgfr2 was significantly up-regulated af-

ter 28 days as compared with the controls (Figures 4K and S10A–S10C). Subsequently, CTX was intramuscularly injected at the same place (Figure 4K), and after 3 days, H&E and immunofluorescence staining of muscle cross-sections showed a significantly lower amount of fibrosis/necrosis in AAV-circFgfr2-OV mice (Figure S10D). AAV-circFgfr2-OV suppressed the accumulation of mononucleated cells in the damaged area (Figure S10D). Meanwhile, we observed that the expression of MyoD and Pax7 was significantly higher in the AAV-circFgfr2-OV group as compared with that in the AAV-circFgfr2-NC group ($P < 0.05$; Figure S10E–S10G). Five days after CTX injection, new myofibres containing centralized nuclei were formed to repair damaged fibres, as expected (Figures 4L and S6). In comparison with the AAV-circFgfr2-NC group, AAV-circFgfr2-OV up-regulated the expression of myogenin in TA muscle and stimulated the growth of new myofibres 5 days following CTX injection (Figure 4K and 4M). An increase in myofibre size was observed in muscle treated with AAV-circFgfr2-OV, whereas abundant mononucleated cells still existed in control muscle (Figures 4N and S10H). The cross-sectional area of newly formed myofibres was significantly larger in the AAV-circFgfr2-OV group than that in the control muscle (Figure 4O). Taken together, these results suggest that circFgfr2 represses the proliferation of myoblasts and promotes myoblast differentiation and muscle regeneration.

circFgfr2 regulates Map3k20 by sponging miR-133

To determine the regulatory mechanism of circFgfr2 in myogenesis and muscle regeneration, we first evaluated miRNAs that had potential binding sites in the circFgfr2 transcript, and 16 miRNAs were predicted by both the TargetScan³⁵ and miRDB³⁶ programs. A luciferase reporter assay was performed in HEK293T cells expressing each of 16 miRNA mimics to validate the interactions. We found that the three miR-133 family members (miR-133a-3p, 133b-3p, and 133c) were the top three miRNAs that significantly reduced the luciferase intensity (Figure 5A and 5C), while they did not inhibit luciferase activity of the reporters with mutated miR-133 binding sites (Figure 5B and 5C). Meanwhile, overexpression of miR-133 significantly reduced the expression of circFgfr2 (Figure 5D), and overexpression of circFgfr2 significantly decreased the abundance of miR-133 (Figure 5E). Next, we conducted Argonaute-2 (Ago2, a core protein of the RISC)-based RIP, followed by RT-qPCR to examine whether Ago2 could pull down circFgfr2 and miR-133 in C2C12 cells. As expected, there was a significant enrichment of circFgfr2 and miR-133 in the Ago2 pull-down samples (Figure 5F), suggesting that circFgfr2 closely interacted with miR-133 via the Ago2 protein. In addition, overexpression of miR-133 could effectively improve the inhibitory effect of circFgfr2 overexpression on myoblast proliferation

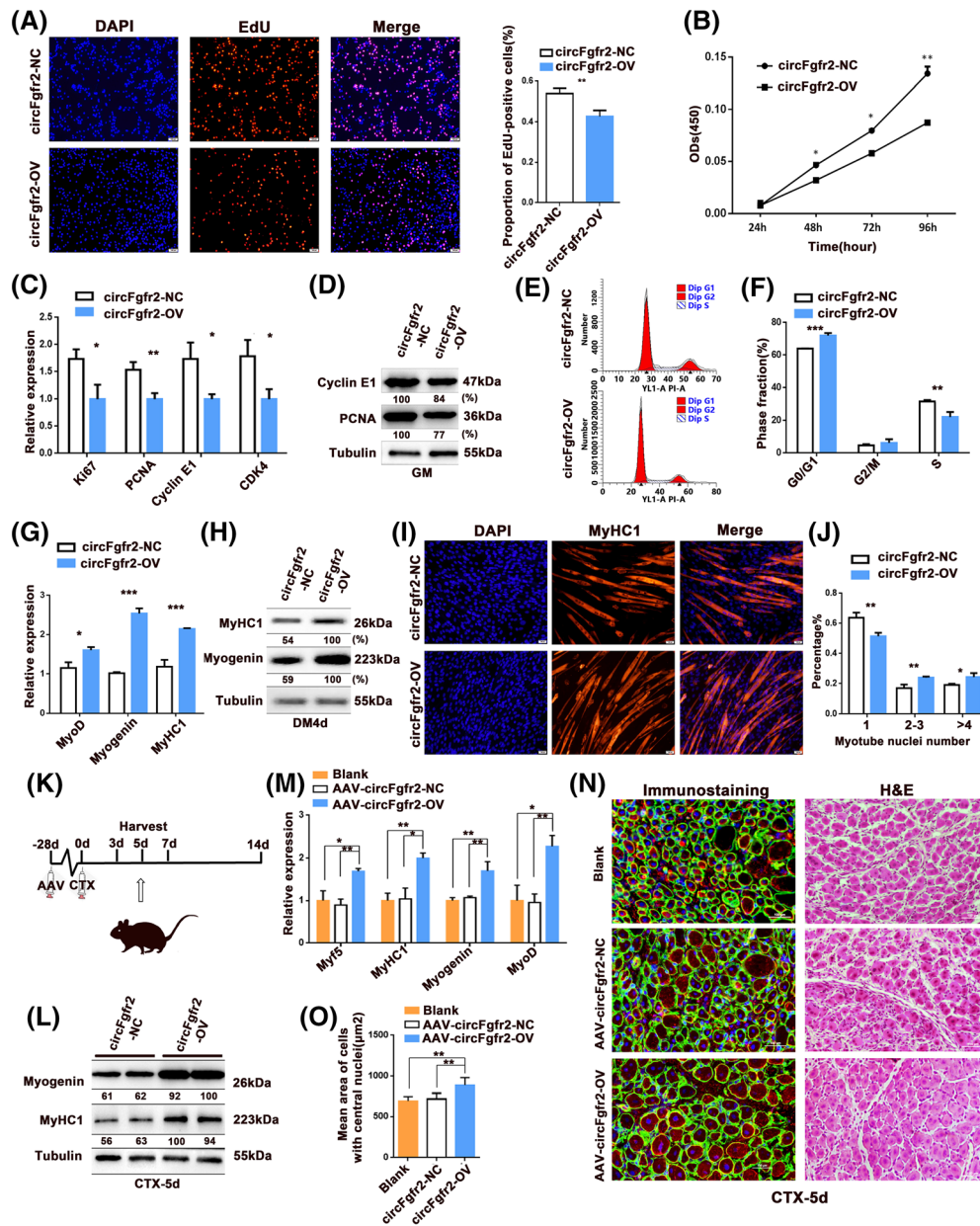


Figure 4 circFgfr2 represses myoblast proliferation and promotes myoblast differentiation and muscle regeneration. (A) EdU assay to assess cell proliferation after transfection with the circFgfr2-overexpression vector (circFgfr2-OV) and negative control (circFgfr2-NC) in proliferating mouse primary myoblasts. Cell proliferation indices were assessed after treatment with EdU and counted using ImageJ. EdU staining (red) for positive cells; DAPI staining (blue) for cell nuclei. (B) Cell proliferation was assessed using the CCK-8 assay after transfection with circFgfr2-OV or circFgfr2-NC vectors in proliferating mouse primary myoblasts. (C and D) The expression of proliferation and cell cycle markers was quantitated by RT-qPCR (C) and western blotting (D) in proliferating mouse primary myoblasts. (E and F) The cell cycle was analysed using flow cytometry after transfection with circFgfr2-OV and their negative controls in proliferating mouse primary myoblasts. The error bars depict the mean \pm SD of samples from three individuals. (G and H) Following transfection of the circFgfr2-OV and their negative controls (circFgfr2-NC), the expression levels of myogenic differentiation markers MyoD, myogenin, and MyHC1 mRNA were detected by RT-qPCR (G) and western blotting (H) in mouse primary myoblasts that differentiated after 4 days. (I) Immunofluorescence microscopy analysis of expression of MyHC1 after transfection with circFgfr2-OV and circFgfr2-NC in mouse primary myoblasts that differentiated after 4 days *in vitro*. The scale bars represent 100 μ m. (J) The number of nuclei per myotube was counted after transfection with circFgfr2-OV and circFgfr2-NC in mouse primary myoblasts that differentiated after 4 days. (K) Injection scheme for AAV-circFgfr2-OV or AAV-circFgfr2-NC into CTX-injured muscles. $N = 5$ per group. (L) RT-qPCR analysis of the expression of Myf5, myogenin, MyHC1, and MyoD in AAV-circFgfr2-OV and AAV-circFgfr2-NC TA muscles on day 5 post-injury. Data are presented as the mean \pm SEM. (M) Western blotting of the expression of myogenin and MyHC1 in AAV-circFgfr2-OV and AAV-circFgfr2-NC TA muscles on day 5 post-injury. (N) Immunostaining (left) and H&E staining (right) for desmin (red) and laminin (green) in AAV-circFgfr2-OV and AAV-circFgfr2-NC TA muscles on day 5 post-injury (scale bar: 100 μ m). (O) Average area of the cross-sections of regenerating fibres on day 5 post-CTX injury. $N = 5$ per group. The error bars depict the mean \pm SD of samples from three to five replicates. * $P < 0.05$ and ** $P < 0.01$.

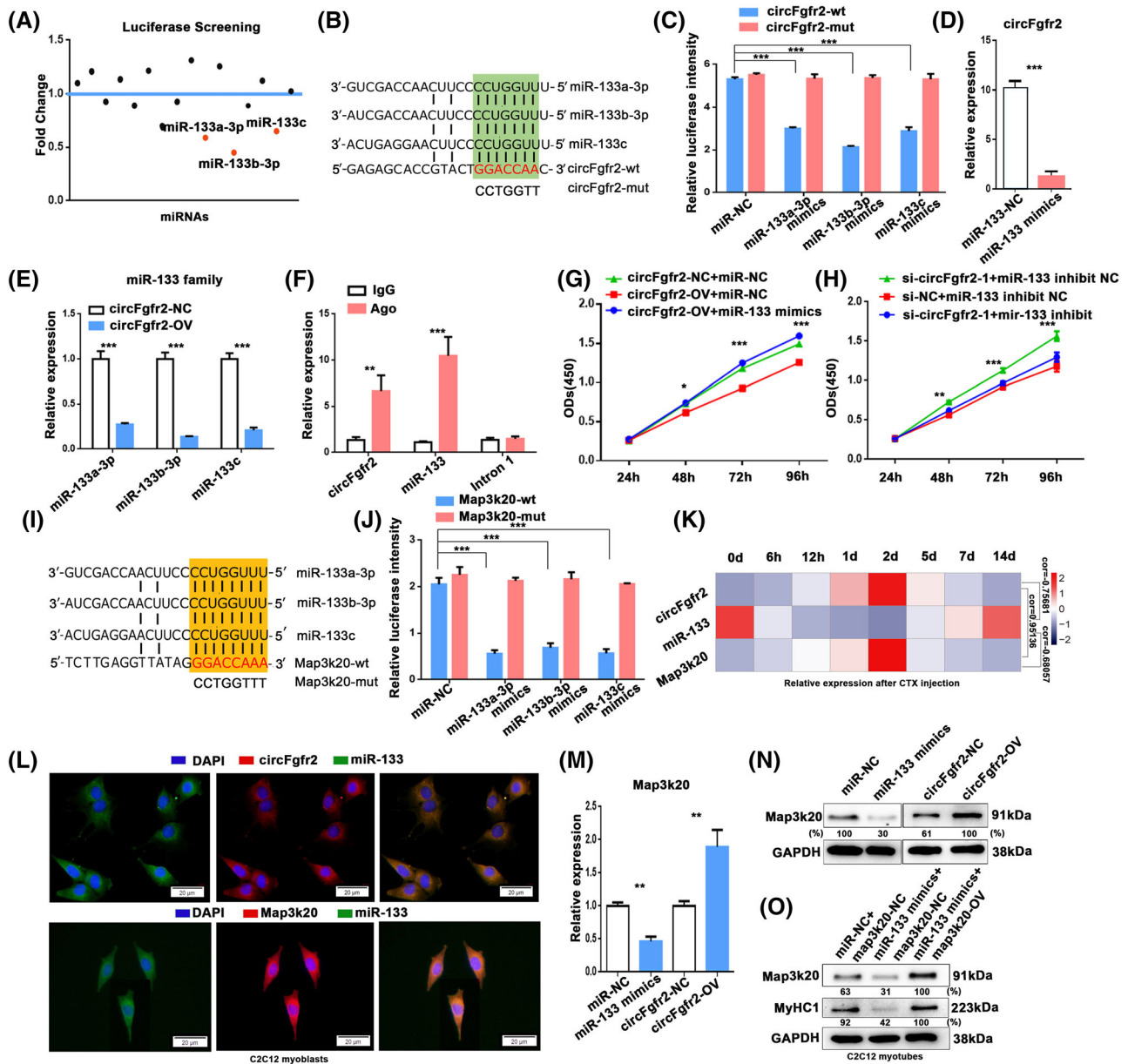


Figure 5 circFgfr2 acts as a ceRNA to promote Map3k20 expression by sponging miR-133 family members. (A) Ratio of Firefly to Renilla luciferase activity following co-transfection with each of 16 miRNA mimics and luciferase reporters containing all circFgfr2 sequences. (B and C) Ratio of Firefly to Renilla luciferase activity following co-transfection with pscheck-circFgfr2-wt/pscheck-circFgfr2-mut and miR-133 mimics/miR-NC. (D) The effects of miR-133 mimics on the expression level of circFgfr2 in C2C12 myoblasts indicated by RT-qPCR. (E) RT-qPCR showing the expression levels of miR-133 family members following transfection with circFgfr2-OV. (F) Fold enrichment of miR-133 and circFgfr2 quantitated by RT-qPCR after the RIP assay with the Ago2 antibody. IgG was used as a negative control for immunoprecipitation, and a sequence snippet from Fgfr2 intron 1 was used as a negative-control region. (G) Effect of miR-133 mimics or their negative control on circFgfr2-OV inhibition of cell proliferation in C2C12 myoblasts by the CCK-8 assay. (H) Effect of miR-133 inhibitors and their negative control on si-circFgfr2-1 promotion of cell proliferation in C2C12 myoblasts by the CCK-8 assay. (I) Schematic illustration of the predicted binding sites for miR-133 family members in the 3'UTR of Map3k20. (J) HEK293T cells were co-transfected with Map3k20 3'UTR or 3'UTR-mut constructs and the miR-133 family mimics. Data were normalized to the Renilla luciferase activity. (K) Heatmap showing the relative expression of circFgfr2, Map3k20, and miR-133 in TA muscles during regeneration after CTX injury. The expression levels of these genes were determined by RT-qPCR. The expression correlation between any two genes were calculated by Pearson correlation coefficient and was shown on the right. (L) An RNA-FISH assay was performed to determine miR-133, Map3k20, and circFgfr2 subcellular localization in proliferating C2C12 myoblasts. Scale bar, 20 μ m. (M and N) RT-qPCR (M) and western blotting (N) of Map3k20 expression in proliferating C2C12 myoblasts transfected with miR-133 mimics or circFgfr2-OV and their negative controls. (O) The expression levels of Map3k20 and MyHC1 proteins in C2C12 myotubes co-transfected with miR-133 mimics and/or the Map3k20-overexpression vector were higher than those in C2C12 myotubes transfected with miR-133 mimics alone as shown by western blotting. The error bars depict the mean \pm SD of samples from three to five measurements. * $P < 0.05$, ** $P < 0.01$, *** $P < 0.001$.

(Figure 5G), and interference with miR-133 mimics inhibited the myoblast proliferation promoting effect of circFgfr2 knockdown (Figure 5H). These findings strongly suggest that circFgfr2 is a direct target of miR-133 family members.

We then explored the mechanism through which the miR-133 family and circFgfr2 regulates myogenesis. Map3k20 was a putative target of miR-133 family members predicted by both the TargetScan³⁵ and miRDB³⁶ programs (Figure 5I). The luciferase reporter assay showed that overexpression of miR-133 significantly repressed the luciferase activity of the wild-type Map3k20 3'UTR reporter, whereas this repression was abolished when the corresponding binding sites were mutated (Figure 5J). During skeletal muscle regeneration, Map3k20 had a negative correlation with miR-133 and a positive correlation with circFgfr2 expression ($P < 0.05$; Figure 5K). Subcellular localization analysis showed that both miR-133 and Map3k20 were mainly distributed in the cytoplasm similar to circFgfr2 (Figure 5L). Meanwhile, overexpression of miR-133 family members resulted in a decrease in the expression of Map3k20, while overexpression of circFgfr2 significantly up-regulated the expression of Map3k20 (Figure 5M and 5N). We observed that overexpression of Map3k20 effectively reversed the inhibitory effect of miR-133 mimics on the expression of MyHC1 (Figure 5O). In addition, consistent with the functions of circFgfr2 in myogenesis, knockdown of Map3k20 inhibited myoblast proliferation and promoted differentiation (Figure S11), whereas opposite effect was observed following Map3k20 overexpression (Figure S11). Collectively, these results show that circFgfr2 acts as an miR-133 family sponge to promote Map3k20 expression during myogenesis and muscle regeneration.

Bulk and single-cell RNA-seq reveal that circFgfr2 regulates the activity of the JNK/MAPK signalling pathway

Map3k20 is one of the upstream factors regulating the JNK/MAPK signalling pathway.³⁷ Given that circFgfr2 regulated Map3k20 expression by sponging miR-133, we hypothesized that circFgfr2 may regulate skeletal muscle development via the JNK/MAPK signalling pathway. To address this, we first examined the global transcriptome changes by poly(A) RNA-seq in proliferating C2C12 cells following the overexpression of circFgfr2. In comparison with the control group, 2798 genes were up-regulated following circFgfr2 overexpression (Figure 6A, Table S6). Enrichment analysis suggested that the up-regulated genes were significantly enriched for GO categories related to the cell cycle and KEGG pathways related to mitogen-activated protein kinase (MAPK) signalling (Figure S12). Key genes of the MAPK signalling pathway were up-regulated (Figure 6B). RT-qPCR analysis validated that genes of the MAPK pathway were up-regulated following circFgfr2 overexpression (Figure 6C).

Meanwhile, western blotting analysis in C2C12 cells indicated that overexpression of circFgfr2 resulted in a marked increase in the expression of Map 3k20, p-MKK7, and p-JNK during both the proliferation (Figure 6D) and differentiation (Figure 6E) phases.

To further demonstrate the regulation of circFgfr2 in the JNK/MAPK pathway, we performed single-cell RNA-seq (scRNA-seq) analysis (10× Genomics) in AAV-circFgfr2-OV-treated muscle 5 days after CTX injection. After quality control, a total of 67 121 cells were retained (Table S7) and 9 cell types were identified by t-SNE clustering and annotated (Figure 6F). Consistent with the enhancing function of circFgfr2 in muscle regeneration, the expression levels of MyoD, Myh4, Myf5, and Pax7 were elevated in muscle stem cells (MuSCs) from the AAV-circFgfr2-OV group as compared with those from the control group (Figure 6G). Meanwhile, overexpression of circFgfr2 activated the expression of Map3k20 and other key genes in the JNK pathway during muscle remodelling in muscle-associated cell types (Figure 6H). These results indicate that circFgfr2 regulates myogenesis and muscle regeneration by activating the JNK/MAPK pathway.

Klf4 targets circFgfr2 via a negative feedback loop

Next, we predicted the transcription factors (TFs) that could potentially bind to the Fgfr2 promoter using JASPAR (<http://jaspar.genereg.net>). Among the predicted TFs, Klf4 caught our attention because it has been reported to promote muscle cell differentiation³⁸ and skeletal muscle regeneration.³⁹ There were multiple putative Klf4 binding motifs in the promoter of circFgfr2 (Figure 7A). We cloned three continuous regions containing these binding sites (B1–B3) and constructed a series of luciferase reporter vectors (Figure 7B). The results showed that Klf4 promoted the luciferase activity of the B2 and B3 promoter but did not affect the B1 promoter (Figure 7C). We constructed Klf4 overexpression vector and confirmed its effect at the protein level (Figure S13A). Overexpression of Klf4 significantly up-regulated the expression of linear Fgfr2 mRNA and circFgfr2 (Figures 7D and S13A). Moreover, ChIP-qPCR analysis demonstrated that Klf4 could bind to the B3 of the circFgfr2 promoter (Figure 7E). These data demonstrate that circFgfr2 is a direct target of Klf4.

Previous studies have shown that activation of JNK signalling and subsequent phosphorylation of Klf4 inhibits the Klf4 transcription and transactivation activity.⁴⁰ Meanwhile, JNK/MAPK signalling pathway was reported to positively regulate myogenic differentiation.⁴¹ Accordingly, in conjunction with our findings, we proposed a circFgfr2-mediated regulatory model of myogenesis in which circFgfr2 is regulated by Klf4 and acts as a decoy for miR-133 to relieve its inhibitory effect on Map3k20 and activate the JNK/MAPK signalling pathway. Activation of JNK signalling inhibits Klf4

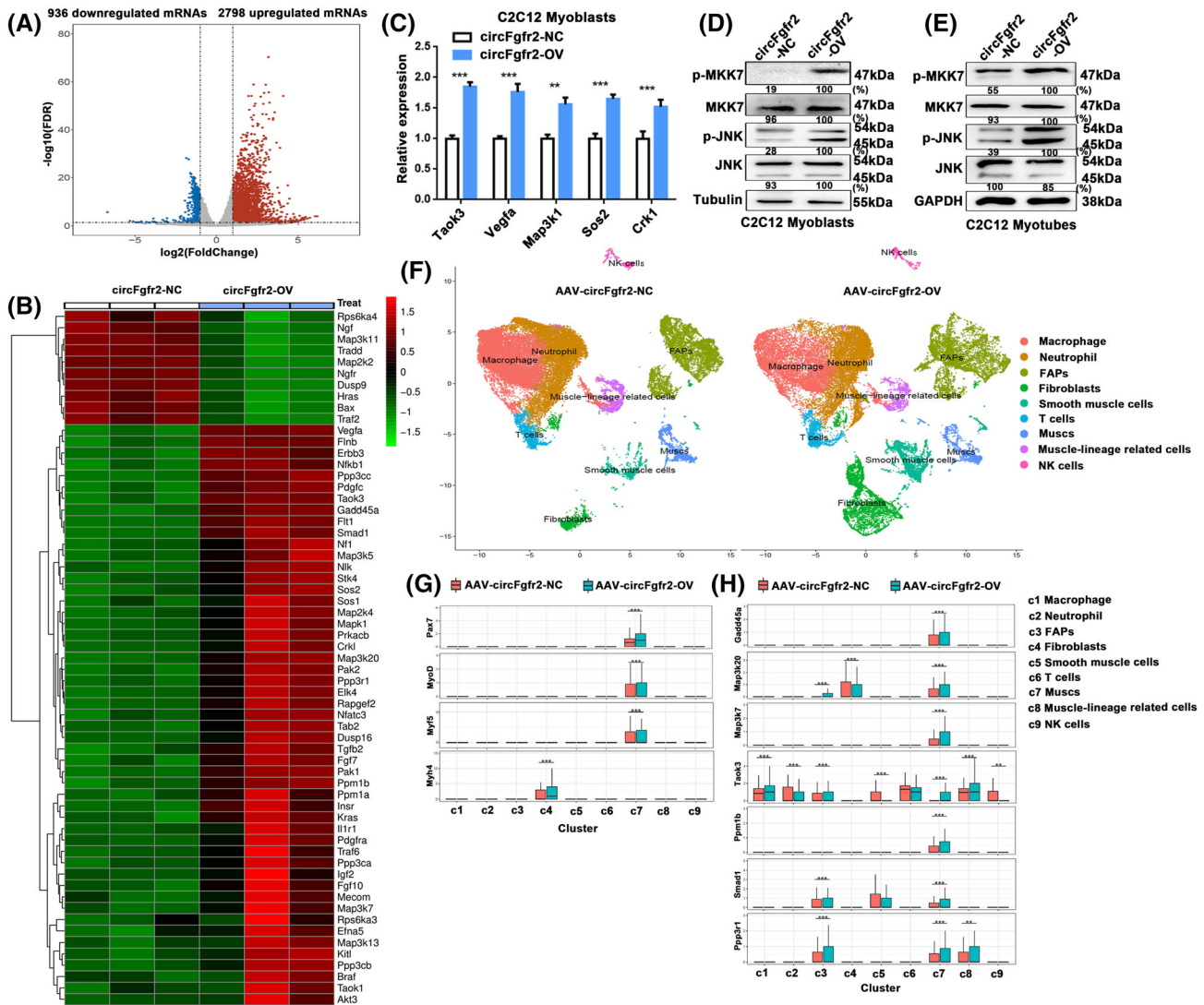


Figure 6 Bulk and single-cell RNA-seq reveal that circFgfr2 regulates the activity of the JNK/MAPK signalling pathway. (A) Volcano plot presents the differentially expressed mRNAs ($|\log_2 \text{fold change}| > 1$ and $\text{FDR} < 0.05$) in circFgfr2-overexpressing C2C12 myoblasts as compared with their negative controls. (B) Heatmap analysis visualized the expression changes of genes in the MAPK signalling pathway following overexpression of circFgfr2. (C) Validation of differentially expressed mRNAs using RT-qPCR. The error bars depict the mean \pm SD of samples from three individuals. ** $P < 0.01$ and *** $P < 0.001$. (D and E) Western blotting showing the expression of genes in the JNK/MAPK pathway following overexpression of circFgfr2 during the proliferation (D) and differentiation (E) stages. (F) Graph-based clustering of FACS-isolated single cells identifies distinct clusters corresponding to different skeletal muscle regeneration cell populations. (G) Expression pattern of MyoD, Myf4, Myf5, and Pax7 in skeletal muscle regeneration cell clusters. (H) The expression pattern of JNK pathway-related genes in skeletal muscle regeneration cell clusters.

transcription and transactivation activity, eventually forming an auto-regulatory feedback loop during myogenesis and muscle regeneration (Figure 7F).

G3bp1 modulates the biogenesis of circFgfr2

To explore the mechanism that mediates the biogenesis of circFgfr2 during skeletal muscle development, we analysed the putative binding sites of RNA binding proteins (RBPs) in the canonical pre-mRNA of circFgfr2. Six putative G3bp1

binding sites, two upstream and four downstream, were predicted (Figure 7G) via catRAPID.⁴² GTPase-activating protein (SH3 domain) binding protein 1 (G3bp1) has been reported to function as an endoribonuclease that selectively targets genes by binding to their consensus sequence. RT-qPCR showed that overexpression of G3bp1 significantly up-regulated the expression of G3bp1 at the mRNA level as expected (Figure S13B) and down-regulated the expression of circFgfr2, linear *Fgfr2* mRNA, and miR-133 family in C2C12 myoblasts (Figures 7H, S13B, and S13C). RIP demonstrated that G3bp1 could bind to circFgfr2 pre-mRNA via

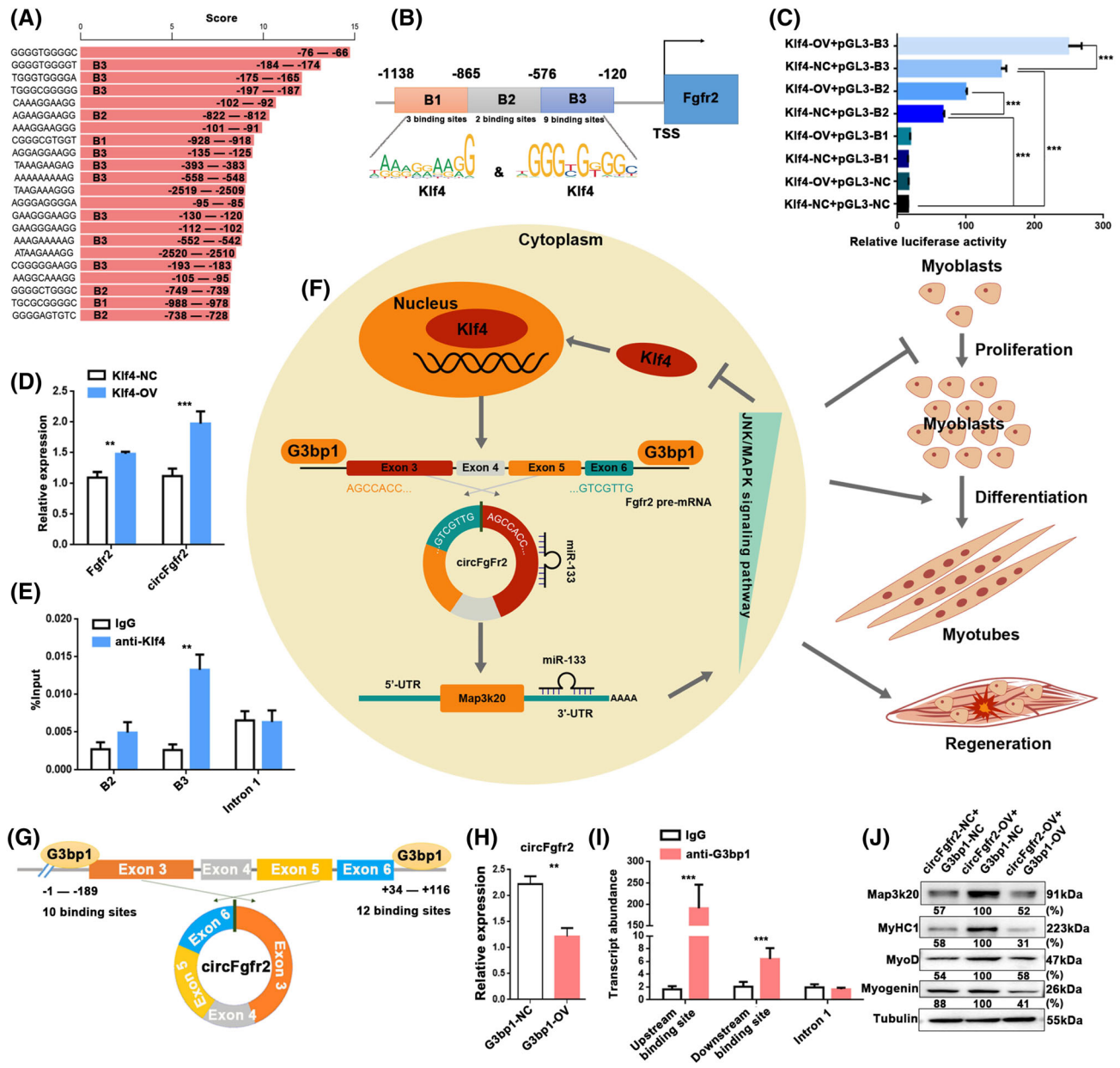


Figure 7 G3bp1 and Klf4 are upstream regulators of circFgfr2. (A) Enriched TF-binding motif Klf4 in the Fgfr2 promoter. (B) Schematic illustration of the sequences of three putative binding regions of Klf4 in the Fgfr2 promoter. (C) The relative luciferase activities were detected in HEK293T cells co-transfected with luciferase reporter plasmids containing binding sites for the promoter sequence and overexpression plasmids of Klf4. HEK293T cells co-transfected with empty pGL3-Basic vector and empty pcDNA3.1 vector were used as negative controls. Firefly luciferase activity was normalized to Renilla luciferase activity. (D) The expression levels of Fgfr2 and circFgfr2 were detected in C2C12 myoblasts transfected with Klf4-overexpression plasmids by RT-qPCR. (E) ChIP-qPCR was performed to determine which putative Klf4 binding site the Fgfr2 promoter was bound in C2C12 myoblasts. IgG was used as a negative control for immunoprecipitation, and a sequence snippet from Fgfr2 intron 1 was used as a negative-control region. The error bars depict the mean \pm SD of samples from three individuals. (F) Schematic diagram illustrating how the mechanism of circFgfr2 mediation by G3bp1 modulates skeletal muscle development via the miR-133/Map3k20/JNK/MAPK/Klf4/circFgfr2 auto-regulatory feedback loop. (G) The putative binding sites of G3bp1 in the upstream and downstream regions of circFgfr2 pre-mRNA were predicted. (H) RT-qPCR analysis of the expression of circFgfr2 following overexpression of G3bp1. (I) RIP confirmed that G3bp1 could directly bind to Fgfr2 pre-mRNA in C2C12 myoblasts. IgG was used as a negative control for immunoprecipitation, and a sequence snippet from Fgfr2 intron 1 was used as a negative-control region. (J) The expression levels of myogenic differentiation markers (MyoD, myogenin, and MyHC1) following co-transfection of the G3bp1-overexpression vector and/or circFgfr2-OV were lower than those following transfection with circFgfr2-OV alone, as shown by western blotting. In (C)–(E), (H), and (I), the error bars depict the mean \pm SD of three replicates. * P < 0.05, ** P < 0.01, *** P < 0.001.

these putative upstream and downstream binding sites using an anti-G3bp1 antibody (Figure 7I). Furthermore, western blotting showed that circFgfr2 overexpression promoted the expression of myoblast differentiation proteins and these effects could be reversed by co-transfection of C2C12 cells with an G3bp1-overexpression vector (Figure 7J). Therefore, G3bp1 binds directly to circFgfr2 and inhibits its biogenesis to modulate muscle development.

Discussion

Accumulating evidence suggests that circRNAs are not simply junk-products of pre-mRNA splicing and points to the potential of circRNAs as novel regulators in a wide range of developmental processes and diseases.^{11–13} Here, we comprehensively profile the dynamic circRNAome atlas of skeletal muscle across 27 developmental stages and identified ~53 000 high-confidence circRNAs in pigs. Approximately 40% of these circRNAs have not been previously identified, which substantially expands the catalogue of circRNAs in mammals.³³

Previous studies have suggested that the function of circRNAs is conserved across species.⁴³ In the present study, we observed that a large proportion of circRNAs are highly conserved across humans, pigs, and mice, suggesting that their functions in myogenesis may also be conserved. Remarkably, we observed that four circRNAs are also up-regulated in differentiated C2C12 myotubes as compared with proliferating myoblasts, which are also differentially expressed during pig skeletal muscle development. Our analytical approach provides an efficient framework to identify conserved circRNAs regulating skeletal muscle development.

To further understand the function and regulatory mechanism of circRNAs during skeletal muscle development, we focused on circFgfr2, which is produced from the Fgfr2 gene. Fgfr2 is an important stimulatory modulator of satellite cells in skeletal muscle and plays a critical role in muscle growth and repair.²⁹ A previous study in chickens has suggested that circFgfr2 promotes myoblast proliferation and differentiation.¹⁸ However, our results reveal that circFgfr2 inhibits myoblast proliferation and promotes differentiation of mouse myoblasts, suggesting that circFgfr2 may have different effects on myoblast proliferation in mammals and chickens. Our results indicate that circFgfr2 is a critical myogenesis regulator during skeletal muscle development and regeneration.

The most well-known functions of circRNAs are as molecular sponges of specific microRNAs and regulators of gene expression via the ceRNA mechanism.¹³ Our results suggest that circFgfr2 acts as a decoy for miR-133 through the ceRNA mechanism to affect the expression of Map3k20. miR-133 is specifically expressed in muscle and has been reported to in-

hibit myoblast differentiation and promote proliferation.⁴⁴ Map3k20 is a member of the MAPKKK family of signal transduction molecules, which forms homodimers to regulate the JNK/MAPK pathway.³⁷ JNK/MAPK signalling pathway plays a positive role in regulating myogenic differentiation.⁴¹ We found that circFgfr2 can activate the JNK/MAPK signalling pathway. In addition, we confirmed that circFgfr2 is regulated by G3bp1 and Klf4. Klf4 belongs to the KLF family of evolutionarily conserved zinc finger TFs that regulate muscle cell differentiation and skeletal muscle regeneration.^{38,39} Interestingly, previous studies have shown activation of JNK signalling and subsequent phosphorylation of Klf4 inhibits the Klf4 transcription.⁴⁰ Therefore, we propose that circFgfr2 is regulated by Klf4 and acts as a ceRNA sponge of miR-133 family members to activate the expression of Map3k20 and the downstream JNK/MAPK signalling pathway. Conversely, the activation of JNK signalling inhibits Klf4 transcription and transactivation activity, establishing an auto-regulatory feedback loop (Figure 7F).

In summary, we profile the first dynamic circRNAome across 27 developmental stages in skeletal muscle and during myoblast differentiation. The present work not only provides a rich circRNA resource for the study of muscle but also outlines a framework for the high-throughput identification of candidate circRNAs associated with skeletal muscle development. We deeply analyse the function and mechanism of conserved circFgfr2 and suggest a circRNA-mediated auto-regulatory feedback loop regulating myogenesis and muscle regeneration, which provides new insight to further understand the regulatory mechanism of circRNAs.

Funding

This work was supported by the National Natural Science Foundation of China (31830090), the Basic and Applied Basic Research Foundation of Guangdong Province (2019B1515120059), the National Key Project (2016ZX08009-003-006), and the Agricultural Science and Technology Innovation Program (CAAS-ZDRW202006).

Acknowledgements

The authors of this manuscript certify that they comply with the ethical guidelines for authorship and publishing in the *Journal of Cachexia, Sarcopenia and Muscle*.⁴⁵

Online supplementary material

Additional supporting information may be found online in the Supporting Information section at the end of the article.

Figure S1. Verification of the reliability of pig circRNAs. Pig circRNAs were validated by PCR with reverse transcription (RT-PCR) using divergent primers following RNase R treatment.

Figure S2. The production and expression of identified circRNAs. (A) Number of circRNAs produced from one gene. (B) The distribution of the sample number per circRNA expressed.

Figure S3. Average read coverage of DNA methylation across gene bodies and the 2-kb regions flanking the BSJ sites of circRNAs at each developmental stage, except E33.

Figure S4. Hierarchical cluster analysis of the skeletal muscle samples. Clustering was performed based on the log₂-transformed CPM values of 3,382 circRNAs that were expressed in at least 80% of samples using the average linkage method by the hclust function in R.

Figure S5. Sequence alignment of the BSJ sequences of circFgfr2 in humans, mice, pigs, and chickens. The BSJ sequences of circFgfr2 in humans (hsa-Fgfr2_0001) were downloaded from the circAtlas database. The BSJ sequence of chicken circFgfr2 was obtained from a previous study [32]. The BSJ sequences of mouse and pig circFgfr2 were amplified in the present study. Sanger sequencing was performed to validate the BSJ sequences of circFgfr2 in the four species.

Figure S6. Construction of the muscle regeneration model following CTX injection in the tibialis anterior (TA). (A) H&E staining of the cross-sections of CTX-induced TA muscle. (B-E) RT-qPCR showing the expression levels of *myogenin*, *MyoD*, *MyHC1*, and *Pax7* during muscle regeneration. The expression level was normalized to 18s-ribosomal RNA. $N = 3-5$ in each group.

Figure S7. Expression patterns of Fgfr2 in mice. (A-B) The expression of Fgfr2 was quantitated by RT-qPCR (A) and western blotting (B) during CTX-induced TA muscle regeneration. (C-D) RT-qPCR (C) and western blotting (D) showing the expression levels of Fgfr2 during C2C12 myogenesis. (E) The expression of Fgfr2 was quantitated by RT-qPCR during postnatal development in the hind leg muscles of C57BL/6 mice. The expression level was normalized to 18s-ribosomal RNA. $N = 3-5$ in each group.

Figure S8. The knockdown and overexpression of circFgfr2 in C2C12 cells and mouse primary myoblasts. (A) Schematic diagram showing the construction of the circFgfr2-overexpression (pLCDH-circFgfr2) vector. (B) RT-qPCR showing the overexpression efficiency of the circFgfr2-overexpression vector in C2C12 cells. (C) RT-qPCR showing the effects of circFgfr2 overexpression on the expression of circFgfr2 and host gene Fgfr2 in mouse primary myoblasts. The error bars depict the mean \pm S.D. of samples from three individuals. $***P < 0.001$. (D) Schematic diagram showing the design of three siRNA oligos against circFgfr2 (si-circFgfr2-1, -2, and -3). (E) RT-qPCR showing the interference efficiency of the three siRNAs in C2C12 myoblasts. (F)

RT-qPCR showing the effect of si-circFgfr2-1 on the expression of circFgfr2 and Fgfr2 in mouse primary myoblasts. The error bars depict the mean \pm S.D. of samples from three individuals. $***P < 0.001$.

Figure S9. Knockdown of circFgfr2 promotes proliferation but prevents differentiation. (A-C) Cell proliferation indices were assessed following treatment with 5-ethynyl-2'-deoxyuridine (EdU) and counted using Image J, after transfection with si-circFgfr2-1 (A) and circFgfr2-OV (B) in proliferating C2C12 myoblasts, and (C) si-circFgfr2-1 in proliferating mouse primary myoblasts. EdU staining (red) for positive cells; DAPI staining (blue) for cell nuclei. The error bars depict the mean \pm S.D. of samples from three individuals. $*P < 0.05$ (D-F) Cell counting kit-8 (CCK-8) assay showing the cell proliferation activity following transfection with si-circFgfr2-1 (D) or circFgfr2-OV (E) in proliferating C2C12 myoblasts, and (F) si-circFgfr2-1 in proliferating mouse primary myoblasts. Data are presented as the mean \pm S.D. of samples from four individuals. $*P < 0.05$, $**P < 0.01$, $***P < 0.001$ (G-H) Transfection of proliferating mouse primary myoblasts with si-circFgfr2-1 and their negative controls. The proliferation and cell cycle markers were quantitated by RT-qPCR (G) and western blotting (H). The error bars depict the mean \pm S.D. of samples from three individuals. $*P < 0.05$ and $**P < 0.01$. (I-J) The cell cycle was analyzed using flow cytometry following transfection with si-circFgfr2-1 and their negative controls in proliferating mouse primary myoblasts. The error bars depict the mean \pm S.D. of samples from three individuals. $*P < 0.05$ and $**P < 0.01$. (K-L) Transfection of mouse primary myoblasts with si-circFgfr2-1 and their negative controls. The mRNA and protein expression levels of myogenic differentiation marker genes (*MyoD*, *myogenin*, and *MyHC1*) were detected by RT-qPCR (K) and western blotting (L) in mouse primary myoblasts that differentiated after 4 days in vitro, respectively. The error bars depict the mean \pm S.D. of samples from three individuals. $*P < 0.05$ and $**P < 0.01$. (M-N) Immunofluorescence analysis of MyHC1 myotubes (M) and the number of nuclei per myotube was counted (N) following knockdown of circFgfr2 in mouse primary myoblasts that differentiated after 4 days in vitro; the scale bars represent 100 μ m.

Figure S10. circFgfr2 promotes skeletal muscle regeneration. (A-C) RT-qPCR (A), H&E staining (B) and fluorescence images (C) showing that injection of AAV-circFgfr2-OV increased circFgfr2 expression in mouse TA muscles 28 days after adenovirus injection. The expression level was normalized to 18s-ribosomal RNA. $**P < 0.01$ post-injury vs. baseline level; $n = 5$ in each group. Data are presented as the mean \pm SEM. (D) H&E staining, Sirius Red staining and immunostaining for desmin (red) and laminin (green) of AAV-circFgfr2-OV and AAV-circFgfr2-NC TA muscles on day 3 post-CTX injury (Scale bar: 50 μ m in H&E staining, Sirius Red staining; 100 μ m in immunostaining). (E-F) RT-qPCR revealing that expression of *Map3k20*, *Pax7*, and *MyoD* was dramatically upregulated

and that of miR-133 was downregulated in AAV-circFgfr2-OV mice on day 3 post-CTX injury. The expression level was normalized to 18s-ribosomal RNA. ** $P < 0.01$ post-injury vs. baseline level; $n = 3-5$ in each group. Data are presented as the mean \pm SEM. **(G)** Western blotting showing the expression of Map3k20, Pax7 and MyoD in AAV-circFgfr2-OV mice on day 3 post-CTX injury. **(H)** Sirius Red staining of AAV-circFgfr2-OV and AAV-circFgfr2-NC TA muscles on day 5 post-CTX injury (Scale bar: 100 μ m).

Figure S11. Map3k20 promotes myoblast differentiation but inhibits proliferation in C2C12 cells. (A-B) RT-qPCR showing the expression of Map3k20 during postnatal skeletal muscle development in mice **(A)** and during C2C12 myoblast myogenesis **(B)**. **(C)** RT-qPCR showing the expression of proliferation markers (*PCNA* and *Ki67*) and myogenic differentiation marker genes (*MyoD*, *myogenin*, and *MyHC1*) following transfection with the Map3k20-overexpression vector in proliferating C2C12 cells. The error bars depict the mean \pm S.D. of samples from three individuals. * $P < 0.05$, ** $P < 0.01$, *** $P < 0.001$. **(D)** RT-qPCR showing the interference efficiency of three Map 3k20 siRNAs (si-Map3k20-1, -2, and -3) and their effect on the expression of *Ki67* and *PCNA* in proliferating C2C12 myoblasts. The error bars depict the mean \pm S.D. of samples from three individuals. * $P < 0.05$, ** $P < 0.01$, *** $P < 0.001$. **(E)** RT-qPCR showing the expression levels of myogenic differentiation marker genes (*MyoD*, *myogenin*, and *MyHC1*) following transfection with si-Map3k20-1 in C2C12 cells that differentiated after 4 days *in vitro*. The error bars depict the mean \pm S.D. of samples from three individuals. * $P < 0.05$, ** $P < 0.01$. **(F)** Western blotting showing the expression levels of *PCNA* and *Cyclin E1* in proliferating C2C12 cells following transfection of Map3k20, si-Map3k20-1, and their negative controls. **(G)** EdU assay to assess cell proliferation after transfection with Map3k20-OV or Map3k20-NC in proliferating C2C12 myoblasts. Cell proliferation indices were assessed after treatment with EdU and counted using Image J. EdU staining (red) for positive cells; Dapi staining (blue) for cell nuclei. The scale bars represent 100 μ m. **(H)** Western blotting showing the expression levels of *myogenin* and *MyHC1* after transfection with Map3k20, si-Map3k20-1, and their negative controls in C2C12 cells that differentiated after 4 days *in vitro*. **(I)** Immunofluorescence

microscopy analysis of expression of *MyHC1* and the number of nuclei per myotube was counted in Map3k20-overexpressing C2C12 cells that differentiated after 4 days *in vitro*. The scale bars represent 100 μ m.

Figure S12. GO and KEGG pathway analyses of differentially expressed genes in circFgfr2-overexpressing circFgfr2 myoblasts as compared with the negative control. (A-B) GO **(A)** and KEGG **(B)** pathway analyses of upregulated genes. **(C-D)** GO **(C)** and KEGG **(D)** pathway analyses of downregulated genes.

Figure S13. Klf4 and G3bp1 modulates the transcription of circFgfr2. (A) Western blotting showing the expression levels of *Klf4* and *Fgfr2* in C2C12 cells following transfection with *Klf4*-OV or *Klf4*-NC. **(B)** The expression level of *G3bp1* and *Fgfr2* in *G3BP1*-overexpressing C2C12 cells. The error bars depict the mean \pm S.D. of samples from three individuals. *** $P < 0.001$. **(C)** The expression level of miR-133 family in *G3BP1*-overexpressing C2C12 cells. The error bars depict the mean \pm S.D. of samples from three individuals. ** $P < 0.01$, *** $P < 0.001$.

Data S1. Detail methods used in the present study.

Table S1. Information regarding the primers used in the present study.

Table S2. Identification of circRNAs in skeletal muscle.

Table S3. The circular junction of circRNAs was identified using divergent primers in Sanger sequencing.

Table S4. Differentially expressed circRNAs during skeletal muscle development in pigs.

Table S5. Differentially expressed circRNAs between differentiated C2C12 myotubes and proliferating myoblasts.

Table S6. Differentially expressed mRNAs in circFgfr2-overexpressing C2C12 myoblasts as compared with their negative controls.

Table S7. Summary of the scRNA-seq data.

Conflict of interest

None declared.

References

- Grefte S, Kuijpers-Jagtman AM, Torensma R, Von den Hoff JW. Skeletal muscle development and regeneration. *Stem Cells Dev* 2007;**16**:857–868.
- Bismuth K, Relaix F. Genetic regulation of skeletal muscle development. *Exp Cell Res* 2010;**316**:3081–3086.
- White RB, Bierinx AS, Gnocchi VF, Zammit PS. Dynamics of muscle fibre growth during postnatal mouse development. *BMC Dev Biol* 2010;**10**:21.
- Le Grand F, Rudnicki MA. Skeletal muscle satellite cells and adult myogenesis. *Curr Opin Cell Biol* 2007;**19**:628–633.
- Buckingham M, Rigby PWJ. Gene regulatory networks and transcriptional mechanisms that control myogenesis. *Dev Cell* 2014;**28**:225–238.
- Charge SB, Rudnicki MA. Cellular and molecular regulation of muscle regeneration. *Physiol Rev* 2004;**84**:209–238.
- Comai G, Tajbakhsh S. Molecular and cellular regulation of skeletal myogenesis. *Curr Top Dev Biol* 2014;**110**:1–73.
- Yu X, Wang Z, Sun H, Yang Y, Li K, Tang Z. Long non-coding MEG 3 is a marker for skeletal muscle development and meat

- production traits in pigs. *Anim Genet* 2018; **49**:571–578.
9. Zhang J, Ying Z, Tang ZL, Long LQ, Li K. MicroRNA-148a promotes myogenic differentiation by targeting the ROCK1 gene. *J Biol Chem* 2012; **287**:21093–21101.
 10. Bai L, Liang R, Yang Y, Hou X, Wang Z, Zhu S, et al. MicroRNA-21 regulates PI3K/Akt/mTOR signaling by targeting TGF β 1 during skeletal muscle development in pigs. *PLoS ONE* 2015; **10**:e0119396.
 11. Salzman J. Circular RNA expression: its potential regulation and function. *Trends Genet* 2016; **32**:309–316.
 12. Qu S, Yang X, Li X, Wang J, Gao Y, Shang R, et al. Circular RNA: a new star of noncoding RNAs. *Cancer Lett* 2015; **365**:141–148.
 13. Memczak S, Jens M, Elefsinioti A, Torti F, Krueger J, Rybak A, et al. Circular RNAs are a large class of animal RNAs with regulatory potency. *Nature* 2013; **495**:333–338.
 14. Vo JN, Cieslik M, Zhang Y, Shukla S, Xiao L, Zhang Y, et al. The landscape of circular RNA in cancer. *Cell* 2019; **176**:869–881, e813.
 15. Veno MT, Hansen TB, Veno ST, Clausen BH, Grebing M, Finsen B, et al. Spatio-temporal regulation of circular RNA expression during porcine embryonic brain development. *Genome Biol* 2015; **16**:245.
 16. Liang G, Yang Y, Niu G, Tang Z, Li K. Genome-wide profiling of *Sus scrofa* circular RNAs across nine organs and three developmental stages. *DNA Res* 2017; **24**:523–535.
 17. Ji P, Wu W, Chen S, Zheng Y, Zhou L, Zhang J, et al. Expanded expression landscape and prioritization of circular RNAs in mammals. *Cell Rep* 2019; **26**:3444–3460, e3445.
 18. Chen X, Ouyang H, Wang Z, Chen B, Nie Q. A novel circular RNA generated by FGFR2 gene promotes myoblast proliferation and differentiation by sponging miR-133a-5p and miR-29b-1-5p. *Cell* 2018; **7**:199.
 19. Wei X, Li H, Yang J, Hao D, Dong D, Huang Y, et al. Circular RNA profiling reveals an abundant circLMO7 that regulates myoblasts differentiation and survival by sponging miR-378a-3p. *Cell Death Dis* 2017; **8**:e3153.
 20. Wang X, Cao X, Dong D, Shen X, Cheng J, Jiang R, et al. Circular RNA TTN acts as a miR-432 sponge to facilitate proliferation and differentiation of myoblasts via the IGF2/PI3K/AKT signaling pathway. *Molecular Therapy-Nucleic Acids* 2019; **18**:966–980.
 21. Li H, Yang J, Wei X, Song C, Dong D, Huang Y, et al. CircFUT10 reduces proliferation and facilitates differentiation of myoblasts by sponging miR-133a. *J Cell Physiol* 2018; **233**:4643–4651.
 22. Li H, Wei X, Yang J, Dong D, Hao D, Huang Y, et al. circFGFR4 promotes differentiation of myoblasts via binding miR-107 to relieve its inhibition of Wnt3a. *Mol Ther Nucleic Acids* 2018; **11**:272–283.
 23. Legnini I, Di Timoteo G, Rossi F, Morlando M, Briganti F, Sthandier O, et al. Circ-ZNF609 is a circular RNA that can be translated and functions in myogenesis. *Mol Cell* 2017; **66**:22–37.
 24. Prather RS. Pig genomics for biomedicine. *Nat Biotechnol* 2013; **31**:122–124.
 25. Groenen MAM, Archibald AL, Uenishi H, Tuggle CK, Takeuchi Y, Rothschild MF, et al. Analyses of pig genomes provide insight into porcine demography and evolution. *Nature* 2012; **491**:393–398.
 26. Yan S, Tu ZC, Liu ZM, Fan NN, Yang HM, Yang S, et al. A huntingtin knockin pig model recapitulates features of selective neurodegeneration in Huntington's disease. *Cell* 2018; **173**:989–1002.
 27. Tang Z, Li Y, Wan P, Li X, Zhao S, Liu B, et al. LongSAGE analysis of skeletal muscle at three prenatal stages in Tongcheng and Landrace pigs. *Genome Biol* 2007; **8**:R115.
 28. Yang Y, Fan X, Yan J, Chen M, Zhu M, Tang Y, et al. A comprehensive epigenome atlas reveals DNA methylation regulating skeletal muscle development. *Nucleic Acids Res* 2021; **49**:1313–1329.
 29. Pawlikowski B, Vogler TO, Gadek K, Olwin BB. Regulation of skeletal muscle stem cells by fibroblast growth factors. *Dev Dyn* 2017; **246**:359–367.
 30. Yang Y, Zhu M, Fan X, Yao Y, Yan J, Tang Y, et al. Developmental atlas of the RNA editome in *Sus scrofa* skeletal muscle. *DNA Res* 2019; **26**:261–272.
 31. Butler A, Hoffman P, Smibert P, Papalexi E, Satija R. Integrating single-cell transcriptomic data across different conditions, technologies, and species. *Nat Biotechnol* 2018; **36**:411–420.
 32. Yang Y, Sun W, Wang R, Lei C, Zhou R, Tang Z, et al. Wnt antagonist, secreted frizzled-related protein 1, is involved in prenatal skeletal muscle development and is a target of miRNA-1/206 in pigs. *BMC Mol Biol* 2015; **16**:4.
 33. Wu W, Ji P, Zhao F. CircAtlas: an integrated resource of one million highly accurate circular RNAs from 1070 vertebrate transcriptomes. *Genome Biol* 2020; **21**:1–14.
 34. Langfelder P, Horvath S. WGCNA: an R package for weighted correlation network analysis. *BMC bioinformatics* 2008; **9**:559.
 35. Agarwal V, Bell GW, Nam JW, Bartel DP. Predicting effective microRNA target sites in mammalian mRNAs. *Elife* 2015; **4**:e05005.
 36. Chen Y, Wang X. miRDB: an online database for prediction of functional microRNA targets. *Nucleic Acids Res* 2020; **48**:D127–D131.
 37. Johnson GL, Lapadat R. Mitogen-activated protein kinase pathways mediated by ERK, JNK, and p38 protein kinases. *Science* 2002; **298**:1911–1912.
 38. Sunadome K, Yamamoto T, Ebisuya M, Kondoh K, Sehara-Fujisawa A, Nishida E. ERK5 regulates muscle cell fusion through Klf transcription factors. *Dev Cell* 2011; **20**:192–205.
 39. Vivien C, Scerbo P, Girardot F, Le Blay K, Demeneix BA, Coen L. Non-viral expression of mouse Oct4, Sox2, and Klf4 transcription factors efficiently reprograms tadpole muscle fibers in vivo. *J Biol Chem* 2012; **287**:7427–7435.
 40. Yao K, Ki MO, Chen H, Cho YY, Kim SH, Yu DH, et al. JNK1 and 2 play a negative role in reprogramming to pluripotent stem cells by suppressing Klf4 activity. *Stem Cell Res* 2014; **12**:139–152.
 41. Zhang X, Sun W, He L, Wang L, Qiu K, Yin J. Global DNA methylation pattern involved in the modulation of differentiation potential of adipogenic and myogenic precursors in skeletal muscle of pigs. *Stem Cell Res Ther* 2020; **11**:536.
 42. Livi CM, Klus P, Delli Ponti R, Tartaglia GG. catRapid signature: identification of ribonucleoproteins and RNA-binding regions. *Bioinformatics* 2016; **32**:773–775.
 43. Arcinas C, Tan W, Fang W, Desai TP, Teh DCS, Degirmenci U, et al. Adipose circular RNAs exhibit dynamic regulation in obesity and functional role in adipogenesis. *Nat Metab* 2019; **1**:688–703.
 44. Chen J-F, Mandel EM, Thomson JM, Wu Q, Callis TE, Hammond SM, et al. The role of microRNA-1 and microRNA-133 in skeletal muscle proliferation and differentiation. *Nat Genet* 2006; **38**:228–233.
 45. von Haehling S, Morley JE, Coats AJS, Anker SD. Ethical guidelines for publishing in the *Journal of Cachexia, Sarcopenia and Muscle*: update 2019. *J Cachexia Sarcopenia Muscle* 2019; **10**:1143–1145.